applied sciences

MDPI

Article

Effect of the Planetesimal Belt on the Dynamics of the Restricted Problem of 2 + 2 Bodies

Govind Mahato [1], Ashok Kumar Pal [2], Sawsan Alhowaity [3], Elbaz I. Abouelmagd [3,4,*] and Badam Singh Kushvah [1]

[1] Department of Mathematics & Computing, Indian Institute of Technology (Indian School of Mines), Dhanbad 826004, Jharkhand, India; gvndmht@gmail.com (G.M.); bskush@iitism.ac.in (B.S.K.)
[2] Department of Mathematics and Statistics, Manipal University Jaipur, Jaipur 303007, Rajasthan, India; ashokpalism@gmail.com or ashok.pal@jaipur.manipal.edu
[3] Department of Mathematics, College of Science & Humanities, Shaqra University, Sahqra 15551, Saudi Arabia; salhowaity@su.edu.sa
[4] Celestial Mechanics and Space Dynamics Research Group (CMSDRG), Astronomy Department, National Research Institute of Astronomy and Geophysics (NRIAG), Helwan, Cairo 11421, Egypt
* Correspondence: elbaz.abouelmagd@nriag.sci.eg or eabouelmagd@gmail.com; Tel.: +20-102-097-6040

Abstract: In this paper, we study the existence and stability of collinear and noncollinear equilibrium points within the frame of the perturbed restricted problem of 2 + 2 bodies by a planetesimal belt. We compare and investigate the corresponding results of the perturbed and unperturbed models. The impact of the planetesimal belt is observed on collinear and noncollinear equilibrium points. We demonstrate that all equilibrium points are unstable, and we numerically investigate the noncollinear equilibrium points. Finally, we emphasize that the proposed problem is a credible model for describing the capture of small bodies by a planet.

Keywords: R2+2BP; planetesimal belt; equilibrium points; stability analysis

check for updates

Citation: Govind, M.; Pal, A.K.; Alhowaity, S.; Abouelmagd, E.I.; Kushvah, B.S. Effect of the Planetesimal Belt on the Dynamics of the Restricted Problem of 2 + 2 Bodies. *Appl. Sci.* **2022**, *12*, 424. https://doi.org/10.3390/app12010424

Academic Editors: Ji Wang, Weiqiu Chen and Bin Huang

Received: 27 November 2021
Accepted: 27 December 2021
Published: 2 January 2022

Publisher's Note: MDPI stays neutral with regard to jurisdictional claims in published maps and institutional affiliations.

1. Introduction

In the field of celestial mechanics, the circular restricted three-body problem (CRTBP), where an infinitesimal body moves under the influence of two primaries without affecting the motion of the primaries, has been extensive used. For details and investigations, see [1–4]. The dynamics of the combined system of two primaries and two minor bodies, called the restricted 2 + 2 body problem (R2+2BP), was analyzed in [5,6]. In this model, two equations of the motion of the CRTBP are coupled with each other by mutual gravitational interactions. This model, or the dual-satellite-like model, helps with studying the dynamic behavior of binary asteroids in the presence of two primaries. Whipple studied R2+2BP and found 14 pairs of equilibrium points [5]. The study of R2+2BP with different disturbing forces produced more precise and accurate data about the system's dynamic behavior.

Many researchers incorporated different effects of R2+2BP to analyze the perturbed dynamics of the system. For example, Kumar et al. studied the generalized R2+2BP by considering the second primary as a straight segment, and showed that length parameter has a subsequent effect on the location of all equilibrium points [7]. Kalvouridis and Mavraganis [8] found R2+2BP dynamics in the presence of the photo gravitational effect, and Kalvouridis [9] studied the impact of oblate in R2+2BP. The families of a periodic orbit in R2+2BP were discussed by Spurgin [10], who found that the orbits are stable. The stability of R2+2BP was evaluated by Milani and Nobili [11], who showed that the integral of the system, which is similar to RTBP, does not result in hill stability. The restricted 2 + 2 problem with a homogeneous axis-symmetric ellipsoid was described by El-Shaboury [12], who also found 16 solutions in the neighborhood of triangular equilibrium points. A ring-shaped disk-like region formed from dust, comets, asteroids, etc., in the space having considerable mass exerts some gravitational force and affects the dynamic behavior of infinitesimal bodies.

In our solar system, the asteroid belt and kuiper belt are dust-belt-like structures. Dust-belt-like structures are also present in the Proxima Centauri system. Many researchers have studied the effect of the asteroid belt in CRTBP [13–16], and found that these perturbations exhibit significant changes in the equilibrium position. In this paper, we investigate some new aspects of R2+2BP, along with the disk-like belt effect on the potential function; as such, we found the change in the equilibrium positions. Moreover, we analyze the variation in the distance of the equilibrium location of a minor body P_1 and P_2 for $\mu_1 = \mu_2$ from its neighboring equilibrium point $L_i, i = 1,2,3,4,5)$ versus mass ratio μ. The effects of perturbed equilibrium points are compared with those of the unperturbed 2 + 2 body problem. We discuss the stability of the perturbed system with the help of eigenvalues for the particle P_1.

In general, the restricted 2 + 2 bodies problem is formulated as a credible model to show the capture of small bodies by a planet. In particular, two primaries are considered to revolve in a circular mutual orbit and two infinitesimal bodies, where neither of them affects the primaries' motion. If the small bodies are temporarily captured in the Hill sphere of the smaller primary, they may become close enough to each other to exchange energy so that one of them becomes regularly and permanently captured. The aforementioned descriptions are considered the major applications of the restricted 2 + 2 bodies problem, which motivated us to study a more generalized model for this problem.

This paper is organized as follows: In Section 2, we formulate the restricted 2 + 2 body problem in the presence of the planetesimal belt effect. In Section 3, the variation in equilibrium points against mass ratio μ is described and we compare the perturbed equilibrium points with unperturbed equilibrium points. Furthermore, a stability analysis is performed in Section 4, and in Section 5, we discuss the results and provide our conclusions.

2. Formulation of the Model

The restricted 2 + 2 body problem consists of two primaries, M_1 and M_2, with unitless masses $1 - \mu$ and μ, respectively. They are assumed to move on circular Keplerian orbits around their common center of mass under their mutual gravitational force. Two infinitesimal bodies, P_1 and P_2, of dimensionless masses μ_1 and μ_2, respectively, move in the gravitational field while mutually attracting each other without perturbing the primaries. The perturbed mean motion n can be considered as in [15–18],

$$n^2 = 1 + \frac{2M_b r_c}{(r_c^2 + T^2)^{\frac{3}{2}}},$$

where M_b is the total mass of the planetesimal belt, and r_c is the dimensionless reference radius of the planetesimal belt. The gravitational potential of the planetesimal-belt-like system is expressed as in [19,20],

$$\varphi_b(R, z) = \frac{M_b}{(R^2 + [a + \sqrt{z^2 + b^2}]^2)^{\frac{1}{2}}},$$

where R is the minor body's radial distance, a is the flatness parameter, b is the core parameter, and z is the coordinate of the planetesimal belt in a direction of Z-axis. The potential reduces to the system of a point mass with the condition $a = b = 0$. Restricting the condition to the XY plane (i.e., $Z = 0$) and defining $T = a + b$, we have the unit less potential written as,

$$\varphi_b(R, 0) = \frac{M_b}{(R^2 + T^2)^{\frac{1}{2}}}.$$

According to the formulation of the restricted 2 + 2 body problem given by [5,21,22], R2 + 2BP is characterized by three parameters, μ, μ_1 and μ_2, which are the mass parameters of M_2, P_1, and P_2, respectively. We consider a perturbed R2+2BP in the rotating coordinate system. Let $(\mu, 0, 0)$, $(\mu - 1, 0, 0)$, (x_1, y_1, z_1), and (x_2, y_2, z_2) be the coordinates of M_1, M_2, P_1, and P_2, respectively, in a rotating frame, as shown in Figure 1.

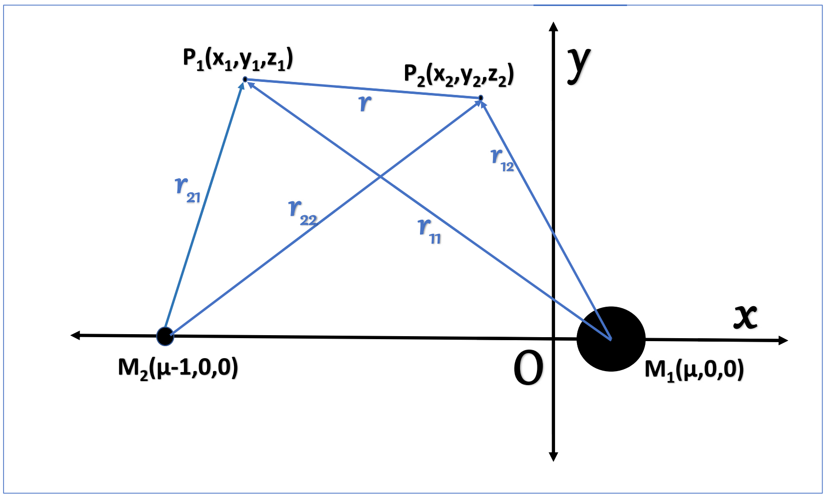

Figure 1. Restricted 2 + 2 body problem model.

Using dimensionless variables and considering the effect of the planetesimal belt, the restricted 2 + 2 problem is described by differential equations [5]:

$$\begin{aligned} \ddot{x}_i - 2n\dot{y}_i &= \frac{1}{\mu_i}\frac{\partial U}{\partial x_i}, \\ \ddot{y}_i + 2n\dot{x}_i &= \frac{1}{\mu_i}\frac{\partial U}{\partial y_i}, \\ \ddot{z}_i &= \frac{1}{\mu_i}\frac{\partial U}{\partial z_i}, \end{aligned} \tag{1}$$

$$U = \sum_{i=1}^{2} \mu_i \left[\frac{1}{2} n^2 \left(x_i^2 + y_i^2 \right) + \frac{1-\mu}{r_{1i}} + \frac{\mu}{r_{2i}} + \frac{1}{2}\frac{\mu_{3-i}}{r} + \frac{M_b}{(R_i^2 + T^2)^{\frac{1}{2}}} \right]. \tag{2}$$

where

$$n^2 = 1 + \frac{2M_b r_c}{(r_c^2 + T^2)^{\frac{3}{2}}}, \quad \mu = \frac{M_2}{M_1 + M_2}, \quad \mu_i = \frac{m_i}{M_1 + M_2}$$

$$r_c^2 = 1 - \mu + \mu^2, \quad R_i^2 = x_i^2 + y_i^2,$$

$$\begin{aligned} r_{1i}^2 &= (x_i - \mu)^2 + y_i^2 + z_i^2, \\ r_{2i}^2 &= (x_i - \mu + 1)^2 + y_i^2 + z_i^2, \\ r^2 &= (x_1 - x_2)^2 + (y_1 - y_2)^2 + (z_1 - z_2)^2. \end{aligned}$$

3. Equilibrium Points

The equilibrium points are the positions of an infinitesimal body where the motion of the minor vanishes. Thus, the velocity and acceleration of $P_i, i = 1, 2$ are zero, i.e., $\dot{x}_i = \dot{y}_i = \dot{z}_i = \ddot{x}_i = \ddot{y}_i = \ddot{z}_i = 0$. Applying these conditions in Equation (2), we obtain,

$$\begin{aligned} U_{x_1} &= \mu_1 \left(n^2 x_1 - \frac{(1-\mu)(x_1-\mu)}{r_{11}^3} - \frac{\mu(x_1-\mu+1)}{r_{21}^3} - \frac{\mu_2(x_1-x_2)}{r^3} \right) \\ &\quad - \frac{M_b x_1}{(R_1^2+T^2)^{\frac{3}{2}}} = 0, \end{aligned} \tag{3}$$

$$U_{y_1} = \mu_1\left(n^2 y_1 - \frac{(1-\mu)y_1}{r_{11}^3} - \frac{\mu y_1}{r_{21}^3} - \frac{\mu_2(y_1-y_2)}{r^3}\right) - \frac{M_b y_1}{(R_1^2+T^2)^{\frac{3}{2}}} = 0, \quad (4)$$

$$U_{z_1} = -\frac{(1-\mu)z_1}{r_{11}^3} - \frac{\mu z_1}{r_{21}^3} - \frac{\mu_2(z_1-z_2)}{r^3} = 0, \quad (5)$$

$$\begin{aligned} U_{x_2} = {} & \mu_2\left(n^2 x_2 - \frac{(1-\mu)(x_2-\mu)}{r_{12}^3} - \frac{\mu(x_2-\mu+1)}{r_{22}^3} - \frac{\mu_1(x_2-x_1)}{r^3}\right) \\ & - \frac{M_b x_2}{(R_2^2+T^2)^{\frac{3}{2}}} = 0, \end{aligned} \quad (6)$$

$$U_{y_2} = \mu_2\left(n^2 y_2 - \frac{(1-\mu)y_2}{r_{12}^3} - \frac{\mu y_2}{r_{22}^3} - \frac{\mu_2(y_2-y_1)}{r^3}\right) - \frac{M_b y_2}{(R_2^2+T^2)^{\frac{3}{2}}} = 0, \quad (7)$$

$$U_{z_2} = -\frac{(1-\mu)z_2}{r_{21}^3} - \frac{\mu z_2}{r_{22}^3} - \frac{\mu_1(z_2-z_1)}{r^3} = 0. \quad (8)$$

Simplifying Equation (5), we obtain,

$$z_1 = z_2 \frac{\mu_2}{r^3\left[\frac{(1-\mu)}{r_{11}^3} + \frac{\mu}{r_{21}^3} + \frac{\mu_2}{r^3}\right]}. \quad (9)$$

Using the value of z_1 from (9) in (8), we obtain either $z_2 = 0$ or $c = 0$, where

$$c = \left[\frac{(1-\mu)}{r_{21}^3} + \frac{\mu}{r_{22}^3} + \frac{\mu_1}{r^3} - \frac{\mu_1\mu_2}{r^6\left\{\frac{(1-\mu)}{r_{11}^3} + \frac{\mu}{r_{21}^3} + \frac{\mu_2}{r^3}\right\}}\right].$$

However, we observe that c is nonzero for all values of μ, μ_1, and μ_2. Therefore, z_2 must be zero and hence $z_1 = 0$. Consequently, all equilibrium points of the restricted 2 + 2 body problem lie on the XY plane. Hence, the solutions of the equilibrium points can be obtained from Equations (3), (4), (6) and (7).

3.1. Collinear Equilibrium Points

The collinear equilibrium points appear on the X-axis. These points can be calculated using Equations (3) and (6) with conditions $y_1 = 0$ and $y_2 = 0$. Then, we have,

$$\begin{aligned} \mu_1\Big(nx_1 - \frac{(1-\mu)(x_1-\mu)}{|x_1-\mu|^3} - \frac{\mu(x_1-\mu+1)}{|x_1-\mu+1|^3} - \frac{\mu_2(x_1-x_2)}{|x_1-x_2|^3}\Big) \\ - \frac{M_b}{x_1^2}\left(1 - \frac{3}{2}\frac{T^2}{x_1^2} + \frac{15}{8}\frac{T^4}{x_1^4}\right) = 0, \end{aligned} \quad (10)$$

$$\begin{aligned} \mu_1\Big(nx_1 - \frac{(1-\mu)(x_1-\mu)}{|x_1-\mu|^3} - \frac{\mu(x_1-\mu+1)}{|x_1-\mu+1|^3} - \frac{\mu_2(x_1-x_2)}{|x_1-x_2|^3}\Big) \\ - \frac{M_b}{x_1^2}\left(1 - \frac{3}{2}\frac{T^2}{x_1^2} + \frac{15}{8}\frac{T^4}{x_1^4}\right) = 0. \end{aligned} \quad (11)$$

The solution of the present model obtained by the perturbation method was proposed by [5]. The solutions of Equations (10) and (11) are x_1 and x_2, expressed in a power series with small parameters [5,8].

$$\begin{aligned} x_1 &= L_j + a_{11}\varepsilon_2 + a_{12}\varepsilon_2^2 + \ldots, \\ x_2 &= L_j + a_{21}\varepsilon_1 + a_{22}\varepsilon_1^2 + \ldots, \end{aligned}$$

where $\varepsilon_i = \dfrac{\mu_i}{(\mu_1+\mu_2)^{\frac{2}{3}}}$ and $L_j, j = 1,2,3$ are the collinear Lagrangian points of CRTBP. Hence, Equations (10) and (11) can be written as:

$$a_{11}W^0_{xx}\varepsilon_2 - \frac{\mu_2(x_1-x_2)}{|x_1-x_2|^3} = 0, \tag{12}$$

$$a_{21}W^0_{xx}\varepsilon_1 - \frac{\mu_1(x_2-x_1)}{|x_1-x_2|^3} = 0, \tag{13}$$

where

$$W = \frac{1}{2}n^2\left(x^2+y^2\right) + \frac{1-\mu}{r_1} + \frac{\mu}{r_2} + \frac{M_b}{(R^2+T^2)^{\frac{1}{2}}}. \tag{14}$$

Using Equations (12) and (13), we have $a_{11} = -a_{21}$ and $a_{11} = \pm\dfrac{1}{(W_{xx})^{\frac{1}{3}}}$. Thus, the equilibrium points of R2+2BP are:

$$L^{P_1}_{j\pm} = L_j \pm \frac{\mu_2}{[(\mu_1+\mu_2)^2 W_{xx}]^{\frac{1}{3}}}, \tag{15}$$

$$L^{P_2}_{j\pm} = L_j \pm \frac{-\mu_1}{[(\mu_1+\mu_2)^2 W_{xx}]^{\frac{1}{3}}}. \tag{16}$$

Equations (15) and (16) yield paired equilibrium positions near the collinear equilibrium points $L_j, j = 1,2,3$ of R2+2BP. We denote the collinear equilibrium points as $L^{P_i}_{j\pm}$, $(i = 1,2.j = 1,2,3)$. Superscript P_i denotes the equilibrium points for an infinitesimal body; P_i, $i = 1,2$ denotes the equilibrium points near L_1, L_2, and L_3. Subscript $j\pm$ denotes the relative position of equilibrium points, where $+$ indicates the right and $-$ indicates the left position with respect to $L_j, j = 1,2,3$. Figure 2 shows the positions of the equilibrium points when $\mu = 0.1$, $\mu_1 = 0.01$, and $\mu_2 = 0.001$ with the planetesimal belt effect $M_b = 3\times10^{-7}$ and parameter $T = 0.11$. The positions of the equilibrium points are shown as P_1 (green) and P_2 (red). In the presence of the planetesimal belt effect, we can observe that the first equilibrium position of P_1 $\left(L^{P_1}_{1-}\right)$ is to the left of L_1. The equilibrium position of P_2 $\left(L^{P_2}_{1+}\right)$ is to the right of L_1. Similarly, the second equilibrium position of P_1, i.e., $\left(L^{P_1}_{1+}\right)$, is to the right of L_1. The equilibrium position of P_2, i.e., $\left(L^{P_2}_{1-}\right)$, is to the left of L_1. As such, we also found four collinear equilibrium points near L_2 and L_3.

The positions of the collinear equilibrium points were also calculated numerically, as shown in Tables 1–3 for $\mu_1 = 10^{-10}$, $\mu_2 = 10^{-12}$, $M_b = 3.7\times10^{-7}$, and $T = 0.11$ with the variation in μ. Table 1 shows that when μ increases $L^{P_1}_{1\pm}$, $L^{P_2}_{1\pm}$ decreases. In Tables 2 and 3, $L^{P_1}_{2\pm}$, $L^{P_2}_{2\pm}$, $L^{P_1}_{3\pm}$, and $L^{P_2}_{3\pm}$ increase with increasing μ. Moreover, we analyzed the effect of the planetesimal belt on R2+2BP. The equilibrium positions of two minor bodies are the same if the masses are equal, i.e., $\mu_1 = \mu_2$. Consequently, the distance from L_j to $L^{P_i}_{j\pm}$ for $i = 1,2$ is equal, i.e., if $d(x,y)$ is the distance between points x and y, then $d(L_j, L^{P_1}_{j\pm}) = d(L_j, L^{P_2}_{j\pm})$. Therefore, we plot the distance versus μ in Figure 2 by considering $M_b = 3.7\times10^{-7}$, $T = 0.11$ and $\mu_1 = \mu_2 = 10^{-2}$; in Figure 3, $d(L_1, L^{P_i}_{1\pm})$ increases as μ increases in $0 < \mu < 0.5$. Concurrently, $d(L_2, L^{P_i}_{2\pm})$, and $d(L_3, L^{P_i}_{3\pm})$ decrease as μ increases from 0 to 0.5.

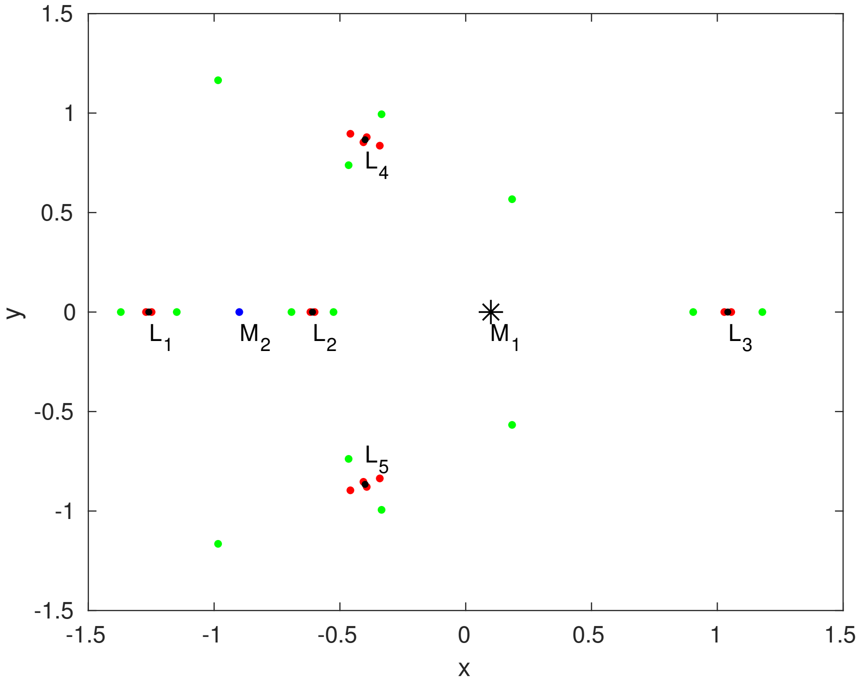

Figure 2. The position of equilibrium points when $\mu = 0.1$, $\mu_1 = 0.01$, $\mu_2 = 0.001$, $M_a = 3 \times 10^{-7}$, and parameter $T = 0.11$. The positions of the primaries are M_1 and M_2, represented by an asterisk and blue dot, respectively. L_1, L_2, L_3, L_4, and L_5 with black dots are the Lagrangian points of CRTBP. The equilibrium points of R2+2BP with the planetesimal belt effect are shown in green and red dots for P_1 and P_2, respectively.

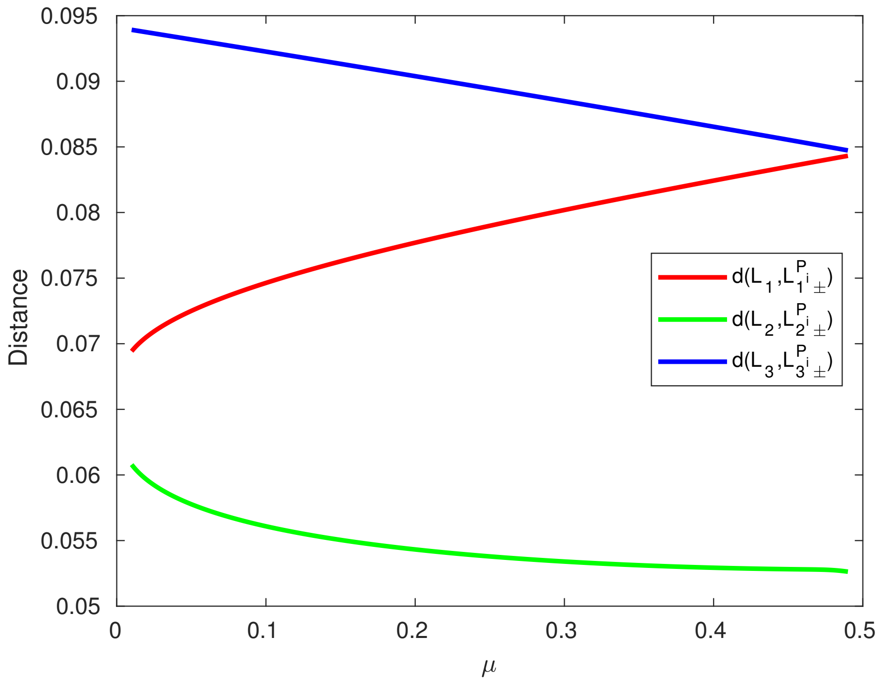

Figure 3. Distance versus mass ratio μ plot in the presence of the planetesimal belt effect for collinear equilibrium points.

Table 1. Equilibrium solution of R2+2BP near L_1.

μ	$L_{1+}^{P_1}$	$L_{1-}^{P_1}$	$L_{1+}^{P_2}$	$L_{1-}^{P_2}$
0.0001	−1.03220039257577	−1.03264998998316	−1.03242743926651	−1.03242294329243
0.0010	−1.06968776321577	−1.07014443189694	−1.06991838089976	−1.06991381421295
0.0100	−1.14652917405563	−1.14700090922027	−1.14676740031377	−1.14676268296213
0.1000	−1.25944627441467	−1.25995339005807	−1.25970236781459	−1.25969729665815

Table 2. Equilibrium solution of R2+2BP near L_2.

μ	$L_{2+}^{P_1}$	$L_{2-}^{P_1}$	$L_{2+}^{P_2}$	$L_{2-}^{P_2}$
0.0001	−0.96784674731841	−0.96828366422587	−0.96806302118760	−0.96806739035667
0.0010	−0.93107229302701	−0.93150165725965	−0.93128482832217	−0.93128912196449
0.0100	−0.84787219955956	−0.84828522573752	−0.84807664751765	−0.84808077777943
0.1000	−0.60884456030787	−0.60922565908104	−0.60903320420059	−0.60903701518832

Table 3. Equilibrium solution of R2+2BP near L_3.

μ	$L_{3+}^{P_1}$	$L_{3-}^{P_1}$	$L_{3+}^{P_2}$	$L_{3-}^{P_2}$
0.0001	1.00036136204178	0.99972197050552	1.00004486323133	1.00003846931597
0.0010	1.00073630603426	1.00009702640224	1.00041986261641	1.00041346982009
0.0100	1.00448569150204	1.00384753168358	1.00416980239190	1.00416342079372
0.1000	1.04192234926276	1.04129546687074	1.04161204247871	1.04160577365479

In Figure 4, we compare the effect of planetesimal belt perturbation on the collinear equilibrium points with unperturbed collinear equilibrium points in consideration of a distance function. In Figure 4a–d, the red line shows the distance $d_1(L_j, L_{j\pm}^{P_i})$, $(j = 1, 2, 3)$ and $(i = 1, 2)$ with the planetesimal belt effect, and the green line shows the distance $d_2(L_j, L_{j\pm}^{P_i})$ without the planetesimal belt effect. Here, d_1 is used to show the effect on distance with planetesimal belt perturbation, whereas d_2 is used for unperturbed collinear points. Figure 4a,d shows that $d_1(L_1, L_{1\pm}^{P_i}) > d_2(L_1, L_{1\pm}^{P_i})$ and $d_1(L_3, L_{3\pm}^{P_i}) > d_2(L_3, L_{3\pm}^{P_i})$ when $0 < \mu < 0.5$. We used a step length $h = 0.001$ for the variation in μ. We found that $d_1(L_2, L_{2\pm}^{P_i}) < d_2(L_2, L_{2\pm}^{P_i})$ for $\mu < 0.153$ and $d_1(L_2, L_{2\pm}^{P_i}) > d_2(L_2, L_{2\pm}^{P_i})$ for $\mu > 0.153$, as shown in Figure 4a–c.

Tables 4–6 show the collinear equilibrium points of the system: Sun–Saturn with the Kuiper belt ($\mu = 0.000286$, $M_b = 3.00 \times 10^{-7}$, $T = 0.11$), Sun–Mars with an asteroid belt ($\mu = 0.0000003$, $M_b = 1.6 \times 10^{-9}$, $T = 0.11$), and the Proxima Centauri system with a dust disc ($\mu = 0.000031$, $M_b = 2.50 \times 10^{-7}$, $T = 0.11$), as described by the authors in [16,23,24] for the restricted 2 + 2 body problem having $\mu_1 = 10^{-10}$ and $\mu_2 = 10^{-12}$. Table 4 shows the equilibrium points near L_1, Table 5 represents the equilibrium points near L_2, and the equilibrium points near L_3 are depicted in Table 6.

Table 4. Equilibrium solution near L_1 of different planetary systems.

μ	$L_{1+}^{P_1}$	$L_{1-}^{P_1}$	$L_{1+}^{P_2}$	$L_{1-}^{P_2}$
0.0002860	−1.04608393024869	−1.04613298051897	−1.04608402825123	−1.04603497798094
0.0000310	−1.02190711476239	−1.02195566697454	−1.02190721176980	−1.02185865955764
0.0000003	−1.00464841079892	−1.00469660080715	−1.00464850708266	−1.00460031707443

Table 5. Equilibrium solution near L_2 of different planetary systems.

μ	$L_{2+}^{P_1}$	$L_{2-}^{P_1}$	$L_{2+}^{P_2}$	$L_{2-}^{P_2}$
0.0002860	−0.95473464120842	−0.95478173944278	−0.95473473531078	−0.95468763707642
0.0000310	−0.97834688228738	−0.97839450372324	−0.97834697743511	−0.97829935599925
0.0000003	−0.99536525492820	−0.99541324652773	−0.99536535081551	−0.99531735921598

Table 6. Equilibrium solution near L_3 of different planetary systems.

μ	$L_{3+}^{P_1}$	$L_{3-}^{P_1}$	$L_{3+}^{P_2}$	$L_{3-}^{P_2}$
0.0002860	1.00011913765467	1.00004978229365	1.00011899908252	1.00018835444353
0.0000310	1.00001290410545	0.99994354530304	1.00001276552642	1.00008212432883
0.0000003	1.00000019376614	0.99993083453848	1.00000005518627	1.00006941441393

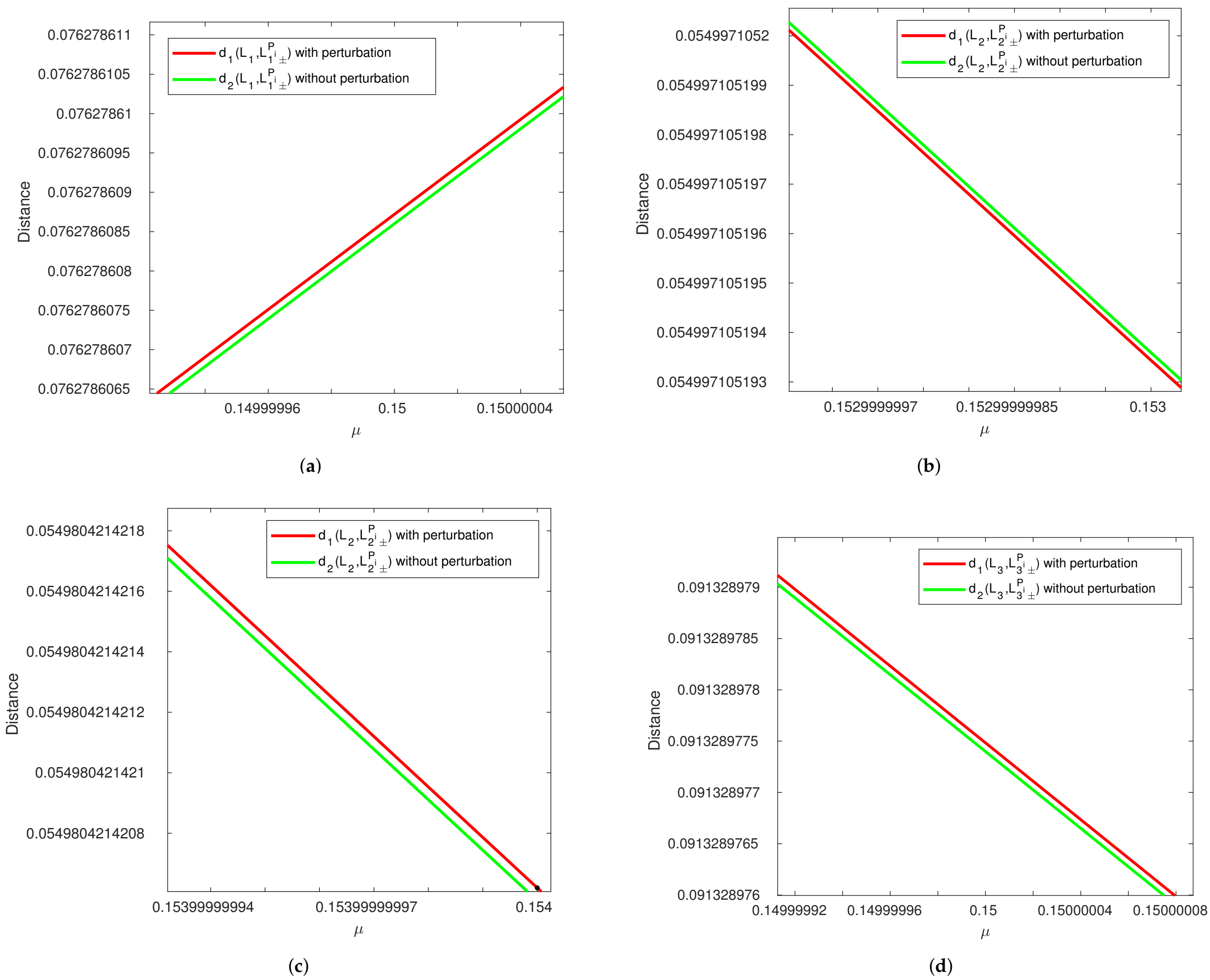

Figure 4. Comparison of distance versus μ between perturbed (red line) and unperturbed (green line) collinear equilibrium points in R2+2BP. (**a**) For L_1 equilibrium point. (**b**) For L_2 equilibrium point. (**c**) For L_2 equilibrium point. (**d**) For L_3 equilibrium point.

3.2. Noncollinear Equilibrium Points

The noncollinear equilibrium points of R2+2BP can be found by solving Equations (3), (4), (6) and (7) with $y_1 \neq 0$ and $y_2 \neq 0$. The solution can be obtained by the power series perturbation method. Let x_i and y_i, $i = 1, 2$ be the solutions; then,

$$x_i = xL_j + a_{i1}\varepsilon_{3-i} + a_{i2}\varepsilon_{3-i}^2 + \dots,$$
$$y_i = yL_j + a_{i1}\varepsilon_{3-1} + a_{i2}\varepsilon_{3-i}^2 + \dots.$$

Solving the above, we obtain

$$x_i^P = \mu - \frac{1}{2} \pm \frac{\alpha_j(-1)^i \mu_{3-i}}{[(\mu_1+\mu_2)^2(W_{xy}\alpha_j + W_{yy})]^{\frac{1}{3}}[1+\alpha_j^2]^{\frac{1}{2}}}, \tag{17}$$

$$y_i^P = \frac{(-1)^{k+1}\sqrt{3}}{2} \pm \frac{\mu_{3-i}}{((\mu_1+\mu_2)^2(W^0_{xy}\alpha_j + W^0_{yy})^{\frac{1}{3}}(1+\alpha_j^2)^{\frac{1}{2}}}, \tag{18}$$

$$x_i^I = \mu - \frac{1}{2} \pm \frac{\alpha_j \mu_{3-i}}{((\mu_1+\mu_2)^2(W^0_{xx} + \frac{W^0_{xy}}{\alpha_j}))^{\frac{1}{3}}(1+\frac{1}{\alpha_j^2})^{\frac{1}{2}}}, \tag{19}$$

$$y_i^I = \frac{(-1)^{k+1}\sqrt{3}}{2} \pm \frac{(-1)^{i+1}\mu_{3-i}}{[(\mu_1+\mu_2)^2(W_{xx} + \frac{W_{xy}}{\alpha_j})]^{\frac{1}{3}}[1+\frac{1}{\alpha_j^2}]^{\frac{1}{2}}}, \tag{20}$$

where, $j = 1, k = 1$ at L_4 and $j = 2, k = 2$ at L_5

$$\alpha_{1,2} = \frac{(-1)^{k+1} \pm (-1)^k\sqrt{1-12(\mu-0.5)}}{2\sqrt{3(\mu-0.5)}}.$$

Equations (17)–(20) represent the noncollinear equilibrium points in R2+2BP. In this section, we use different notations to represent equilibrium points near L_4 and L_5. The prefixes x and y are used in $L^{P_i}_{j\pm}$ to denote the X and Y coordinates of equilibrium points, respectively. The noncollinear equilibrium points can be distinguished as the perpendicular and inline equilibrium solutions in [9]. Again, the prefixes I and P are used for inline and perpendicular equilibrium points, i.e., $IxL^{P_1}_{4-}$ is the X-coordinate of the equilibrium point of the first infinitesimal body toward the origin.

The distance versus μ of the perpendicular and inline equilibrium positions to $L_{4,5}$ with the planetesimal belt effect $M_b = 3.7 \times 10^{-7}$, $T = 0.11$ and $\mu_1 = \mu_2 = 10^{-2}$ are shown in Figure 5a,b. In the case of the perpendicular equilibrium position $d(L_{4,5}, PL^{P_i}_{4,5\pm})$ increases as μ increases, as shown in Figure 5a. In Figure 5b, in the case of the inline equilibrium position, the distance $d(L_{4,5}, IL^{P_i}_{4,5\pm})$ increases rapidly when μ approaches $\frac{1}{2}$. Figure 6a shows that $d_1(L_{4,5}, PL^{P_i}_{4,5\pm}) > d_2(L_{4,5}, PL^{P_i}_{4,5\pm})$, i.e., due to perturbation, the distance increases with respect to the unperturbed distance in the case of perpendicular noncollinear equilibrium points. Here, we use d_1 and d_2 for the perturbed and unperturbed distances, respectively. Furthermore, when the noncollinear equilibrium points are in the perpendicular position, $d_1(L_{4,5}, IL^{P_i}_{4,5\pm}) > d_2(L_{4,5}, IL^{P_i}_{4,5\pm})$, as shown in Figure 6b. Hence, we concluded that the distance increases due to the perturbation.

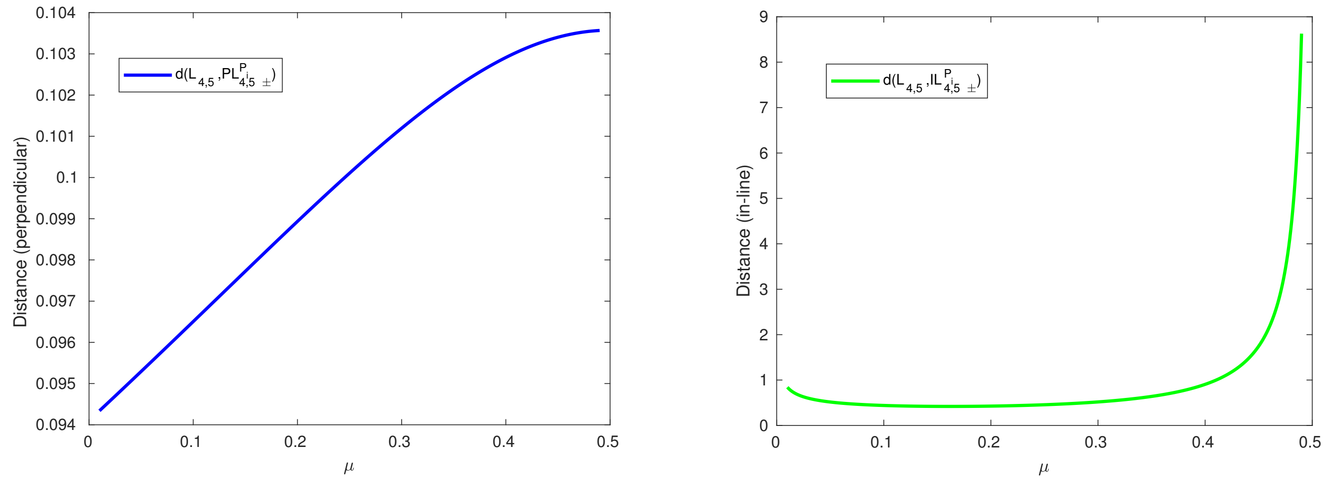

(**a**) (**b**)

Figure 5. Distance versus μ in the presence of the planetesimal belt effect for noncollinear equilibrium points. (**a**) Perpendicular equilibrium points. (**b**) Inline equilibrium points.

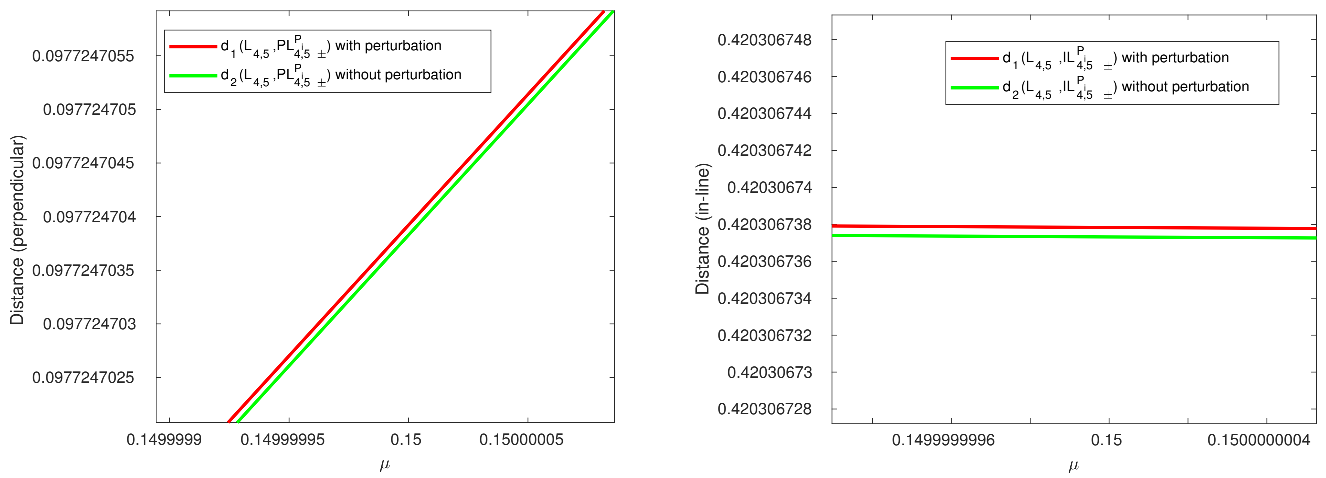

(**a**) (**b**)

Figure 6. Comparison of distance versus μ between perturbed (red line) and unperturbed (green line) noncollinear equilibrium points in R2+2BP. (**a**) Perpendicular equilibrium points. (**b**) Inline equilibrium points.

The positions of the noncollinear equilibrium points were calculated numerically and are shown in Tables 7–10 for $\mu_1 = 10^{-10}$, $\mu_2 = 10^{-12}$, $M_b = 3.7 \times 10^{-7}$, and $T = 0.11$. Table 7 shows the perpendicular equilibrium points, where the coordinates were taken as $(PxL_{4-}^{P_i}, PyL_{4-}^{P_i})$ and $(PxL_{4+}^{P_i}, PyL_{4+}^{P_i})$, $i = 1, 2$. We observed that the coordinates $PxL_{4+}^{P_i}$, $PyL_{4+}^{P_i}$, and $PxL_{4-}^{P_i}$ increased, and $PyL_{4-}^{P_i}$ decreased as we increased the value of μ. The inline equilibrium points $(IxL_{4-}^{P_i}, IyL_{4-}^{P_i})$ and $(IxL_{4+}^{P_i}, IyL_{4+}^{P_i})$ are shown in Table 8.

Furthermore, we observed that $IxL_{4-}^{P_i}$, $IyL_{4-}^{P_i}$, and $IxL_{4+}^{P_i}$ increased as μ increased, whereas $IyL_{4+}^{P_i}$ decreased as μ increased. Table 9 represents the perpendicular equilibrium points near L_5, and $(PxL_{5+}^{P_i}\ PyL_{5+}^{P_i})$ and $(PxL_{5-}^{P_i}, PyL_{5-}^{P_i})$ are coordinates in which $PxL_{5-}^{P_i}$, $PyL_{5-}^{P_i}$, and $PxL_{5+}^{P_i}$ increased and $PyL_{5+}^{P_i}$ decreased as μ increased. Finally, the coordinates of the inline equilibrium points are shown in Table 10. $(IxL_{5+}^{P_i}, IyL_{5+}^{P_i})$ and $(IxL_{5-}^{P_i}, IyL_{5-}^{P_i})$

are the coordinates, and we observed that $IxL_{5+}^{P_i}$, $IyL_{5+}^{P_i}$) and ($IxL_{5-}^{P_i}$) increased and $IyL_{5-}^{P_i}$ decreased as the value of μ increased.

Table 7. Perpendicular equilibrium solution of the restricted 2 + 2 body problem near L_4.

μ	$PxL_{4-}^{P_1}$ $PxL_{4-}^{P_2}$	$PyL_{4-}^{P_1}$ $PyL_{4-}^{P_2}$	$PxL_{4+}^{P_1}$ $PxL_{4+}^{P_2}$	$PyL_{4+}^{P_1}$ $PyL_{4+}^{P_2}$
0.0001	−0.49990159842961	0.86602249507265	−0.49989840157039	0.86602803274910
	−0.50005984296138	0.86574838008869	−0.49974015703862	0.86630214773306
0.0010	−0.49900159770815	0.86602249376500	−0.49899840229185	0.86602803393550
	−0.49915977081539	0.86574825532526	−0.49884022918461	0.86630227237524
0.0100	−0.49000159029866	0.86602248059246	−0.48999840970134	0.86602804590512
	−0.49015902986560	0.86574699761614	−0.48984097013440	0.86630352888144
0.1000	−0.40000149309951	0.86602233889207	−0.39999850690049	0.86602817663806
	−0.40014930995065	0.86573337046563	−0.39985069004935	0.86631714506449

Table 8. In-ine equilibrium solution of the restricted 2 + 2 body problem near L_4.

μ	$IxL_{4-}^{P_1}$ $IxL_{4-}^{P_2}$	$IyL_{4-}^{P_1}$ $IyL_{4-}^{P_2}$	$IxL_{4+}^{P_1}$ $IxL_{4+}^{P_2}$	$IyL_{4+}^{P_1}$ $IyL_{4+}^{P_2}$
0.0001	−0.49978629067686	0.86595962036838	−0.50001370932314	0.86609090745337
	−0.48852906768613	0.85946090966168	−0.51127093231387	0.87258961816007
0.0010	−0.49894714879015	0.86599478074186	−0.49905285120985	0.86605574695864
	−0.49371487901505	0.86297695301132	−0.50428512098495	0.86907357468918
0.0100	−0.48997516675820	0.86601107095682	−0.49002483324180	0.86603945554077
	−0.48751667582044	0.86460603405128	−0.49248332417956	0.86744449244630
0.1000	−0.39998667432169	0.86601844124247	−0.40001332567831	0.86603207428765
	−0.39866743216923	0.86534360550600	−0.40133256783077	0.86670691002412

Table 9. Perpendicular equilibrium solution of the restricted 2 + 2 body problem near L_5.

μ	$PxL_{5+}^{P_1}$ $PxL_{5+}^{P_2}$	$PyL_{5+}^{P_1}$ $PyL_{5+}^{P_2}$	$PxL_{5-}^{P_1}$ $PxL_{5-}^{P_2}$	$PyL_{5-}^{P_1}$ $PyL_{5-}^{P_2}$
0.0001	−0.49989840157039	−0.86602803274910	−0.49990159842961	−0.86602249507265
	−0.49974015703862	−0.86630214773306	−0.50005984296138	−0.86574838008869
0.0010	−0.49899840229185	−0.86602803393550	−0.49900159770815	−0.86602249376500
	−0.49884022918461	−0.86630227237524	−0.49915977081539	−0.86574825532526
0.0100	−0.48999840970134	−0.86602804590512	−0.49000159029866	−0.86602248059246
	−0.48984097013440	−0.86630352888144	−0.49015902986560	−0.86574699761614
0.1000	−0.39999850690049	−0.86602817663806	−0.40000149309951	−0.86602233889207
	−0.39985069004935	−0.86631714506449	−0.40014930995065	−0.86573337046563

Table 10. The inline equilibrium solution of the restricted 2 + 2 body problem near L_5.

μ	$IxL_{5+}^{P_1}$ $IxL_{5+}^{P_2}$	$IyL_{5+}^{P_1}$ $IyL_{5+}^{P_2}$	$IxL_{5-}^{P_1}$ $IxL_{5-}^{P_2}$	$IyL_{5-}^{P_1}$ $IyL_{5-}^{P_2}$
0.0001	−0.50001370932314	−0.86609090745337	−0.49978629067686	−0.86595962036838
	−0.51127093231387	−0.87258961816007	−0.48852906768613	−0.85946090966168
0.0010	−0.49905285120985	−0.86605574695864	−0.49894714879015	−0.86599478074186
	−0.50428512098495	−0.86907357468918	−0.49371487901505	−0.86297695301132
0.0100	−0.49002483324180	−0.86603945554077	−0.48997516675820	−0.86601107095682
	−0.49248332417956	−0.86744449244630	−0.48751667582044	−0.86460603405128
0.1000	−0.40001332567831	−0.86603207428765	−0.39998667432169	−0.86601844124247
	−0.40133256783077	−0.86670691002412	−0.39866743216923	−0.86534360550600

4. Stability of Motion Near Equilibrium Points

We found four paired equilibrium positions around each of L_4 and L_5. In this section, we analyze the stability of the infinitesimal body P_1. Let (x_0, y_0) be any equilibrium point of particle P_1, and δ and ζ be small perturbations in the x and y directions, respectively, i.e., $x_1 = x_0 + \delta$ and $y_1 = y_0 + \zeta$,

$$\ddot{\delta} - 2n\dot{\zeta} = \frac{1}{\mu_1} U_{x_1}(x_0 + \delta, y_0 + \zeta) = \frac{1}{\mu_1}(\delta U^0_{x_1x_1} + \zeta U^0_{x_1y_1}), \tag{21}$$

$$\ddot{\zeta} + 2n\dot{\delta} = \frac{1}{\mu_1} U_{y_1}(x_0 + \delta, y_0 + \zeta) = \frac{1}{\mu_1}(\delta U^0_{y_1x_1} + \zeta U^0_{y_1y_1}). \tag{22}$$

The equations can be written in matrix form as $\dot{X} = AX$, i.e.,

$$\begin{bmatrix} \dot{\delta} \\ \dot{\zeta} \\ \ddot{\delta} \\ \ddot{\zeta} \end{bmatrix} = \begin{bmatrix} 0 & 0 & 1 & 0 \\ 0 & 0 & 0 & 1 \\ \frac{1}{\mu_1} U^0_{x_1x_1} & \frac{1}{\mu_1} U^0_{x_1y_1} & 0 & 2n \\ \frac{1}{\mu_1} U^0_{x_1y_1} & \frac{1}{\mu_1} U^0_{y_1y_1} & -2n & 0 \end{bmatrix} \begin{bmatrix} \delta \\ \zeta \\ \dot{\delta} \\ \dot{\zeta} \end{bmatrix}$$

The characteristic equation of the matrix may be reduced to

$$\lambda_1^4 + (4n^2 - \frac{1}{\mu_1} U^0_{x_1x_1} - \frac{1}{\mu_1} U^0_{y_1y_1})\lambda_1^2 + \frac{1}{\mu_1^2}(U^0_{x_1x_1} U^0_{y_1y_1} - {U^0_{y_1x_1}}^2) = 0. \tag{23}$$

Solving Equation (23), we have,

$$\lambda_{1,2} = \pm \left(\frac{b - \sqrt{b^2 - 4c}}{2} \right)^{\frac{1}{2}}, \tag{24}$$

$$\lambda_{3,4} = \pm \left(\frac{b + \sqrt{b^2 - 4c}}{2} \right)^{\frac{1}{2}}, \tag{25}$$

where, $b = 4n_1^2 - \frac{1}{\mu_1} U^0_{x_1x_1} - \frac{1}{\mu_1} U^0_{y_1y_1}$ and $c = \frac{1}{\mu_1^2}(U^0_{x_1x_1} U^0_{y_1y_1} - {U^0_{y_1x_1}}^2)$.

We note that Equations (24) and (25) are the eigenvalues of the characteristic Equation (23). With the help of these eigenvalues, we can find the stability of particle P_1.

4.1. Stability at Collinear Points

The stability of the collinear equilibrium point of R2+2BP can be approximated by Equation (23), with condition $y_1 = y_2 = 0$, i.e.,

$$\begin{aligned} U^0_{x_1x_1} &= \mu_1 \left(n + \frac{2(1-\mu)}{|x_1 - \mu|^3} + \frac{2\mu}{|x_1 - \mu + 1|^3} + \frac{\mu_2}{|x_1 - x_2|^3} \right) + \frac{3M_b x_1^2}{(T^2 + x_1^2)^{\frac{5}{2}}} \\ &\quad - \frac{M_b}{(T^2 + x_1^2)^{\frac{3}{2}}}, \end{aligned} \tag{26}$$

$$U^0_{y_1y_1} = \mu_1 \left(n - \frac{(1-\mu)}{|x_1 - \mu|^3} - \frac{\mu}{|x_1 - \mu + 1|^3} - \frac{\mu_2}{|x_1 - x_2|^3} \right) - \frac{M_b}{(T^2 + x_1^2)^{\frac{3}{2}}}, \tag{27}$$

and

$$U^0_{x_1y_1} = 0, \tag{28}$$

for $i = 1$. Consequently, $b^2 - 4c > 0$, and hence, the characteristic equation yields at least one positive real root. This results in the instability at the collinear points.

Tables 4–6 provide the collinear equilibrium points for the following systems: Sun–Saturn with the Kuiper belt, Sun–Mars with an asteroid belt, and the Proxima Centauri system with a dust disc. With the help of these collinear equilibrium points, we calculated the stability of these systems using Equations (23)–(28). We found that real nonzero eigenvalues occur with opposite signs and purely imaginary eigenvalues with opposite signs. Thus, the collinear equilibrium points have a saddle×center behavior [25], i.e., all collinear equilibrium points are unstable. Again, as shown in Figure 7, we selected the Sun–Saturn system with the Kuiper belt with $\mu_1 = 10^{-7}$, and plotted the eigenvalues against $\mu_2 \in (10^{-10}, 10^{-7})$. Continuous lines indicate the nonzero real parts of eigenvalues, denoted as α, and the dashed lines represent the nonzero imaginary parts of eigenvalues, denoted as β. Figure 7a,b presents the stability near L_1, Figure 7b,e displays the stability near L_2, and the stability near L_3 is shown in Figure 7c,f. We can observe that all figures have a nonzero positive α, and thus all collinear points are unstable in the considered system.

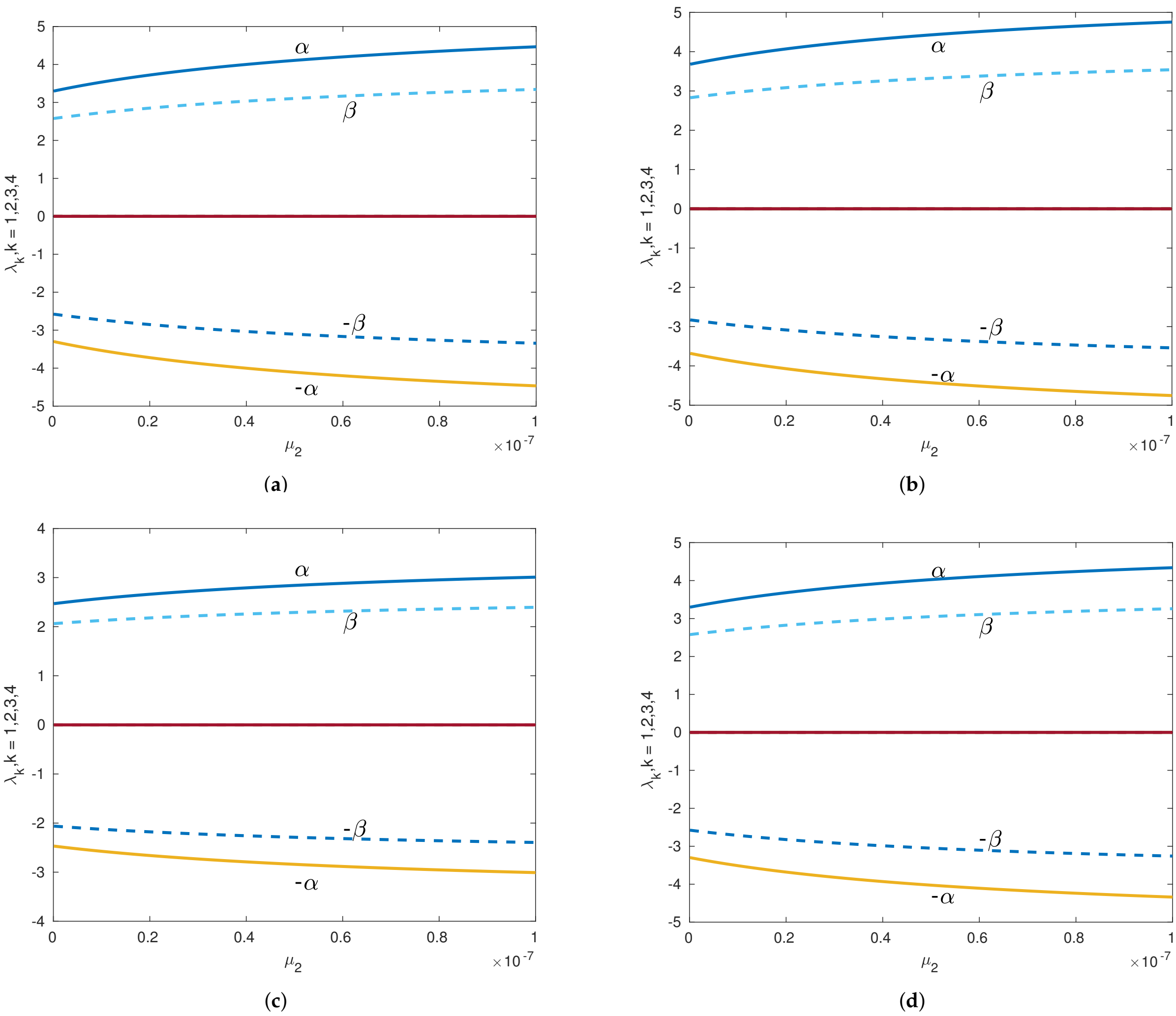

Figure 7. *Cont.*

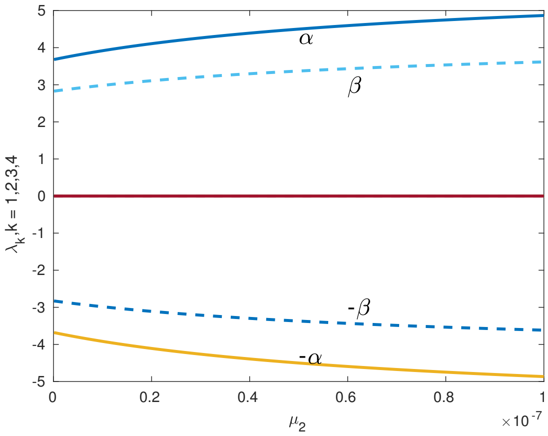

(e)

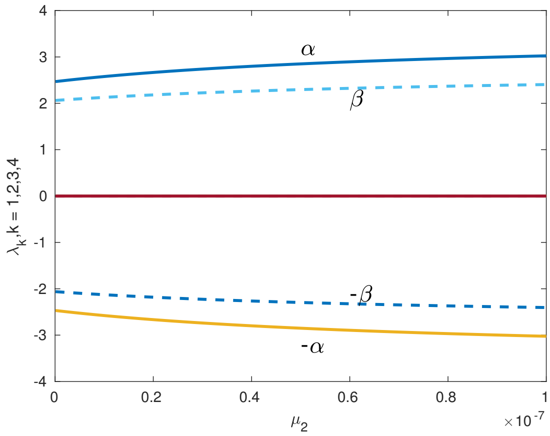

(f)

Figure 7. Eigenvalues versus $\mu_2 \in (10^{-10}, 10^{-7})$ of the Sun–Saturn system in the presence of the Kuiper belt effect for collinear equilibrium points with $\mu_1 = 10^{-7}$. Continuous lines indicate the real parts of the eigenvalues, and dashed lines denote the imaginary parts of the eigenvalues for collinear points. (**a**) Eigenvalues versus μ_2 of equilibrium point left to L_1. (**b**) Eigenvalues versus μ_2 of equilibrium point right to L_1. (**c**) Eigenvalues versus μ_2 of equilibrium point left to L_2. (**d**) Eigenvalues versus μ_2 of equilibrium point right to L_2. (**e**) Eigenvalues versus μ_2 of equilibrium point left to L_3. (**f**) Eigenvalues versus μ_2 of equilibrium point right to L_3.

4.2. Stability at Noncollinear Points

The stability of the triangular restricted problem of 2 + 2 bodies may be approximated by Equation (23), which is calculated for $i = 1$ with the help of the following equations:

$$\begin{aligned} U^0_{x_1x_1} &= \mu_1\left(n + \frac{3(1-\mu)(x_1-\mu)^2}{((x_1-\mu)^2+y_1^2)^{\frac{5}{2}}} - \frac{1-\mu}{((x_1-\mu)^2+y_1^2)^{\frac{3}{2}}} + \frac{3\mu(x_1-\mu+1)^2}{((x_1-\mu+1)^2+y_1^2)^{\frac{5}{2}}}\right. \\ &- \left.\frac{\mu}{((x_1-\mu+1)^2+y_1^2)^{\frac{3}{2}}}\right) + \frac{3\mu_1\mu_2(x_1-x_2)^2}{((x_1-x_2)^2+(y_1-y_2)^2)^{\frac{5}{2}}} \\ &- \frac{\mu_1\mu_2}{((x_1-x_2)^2+(y_1-y_2)^2)^{\frac{3}{2}}} + \frac{3M_bx_1^2}{(T^2+x_1^2+y_1^2)^{\frac{5}{2}}} - \frac{M_b}{(T^2+x_1^2+y_1^2)^{\frac{3}{2}}}, \end{aligned} \tag{29}$$

$$\begin{aligned} U^0_{x_1y_1} &= \mu_1\left(\frac{3(1-\mu)(x_1-\mu)y_1}{((x_1-\mu)^2+y_1^2)^{\frac{5}{2}}} + \frac{3\mu(x_1-\mu+1)y_1}{((x_1-\mu+1)^2+y_1^2)^{\frac{5}{2}}}\right) \\ &+ \frac{3\mu_1\mu_2(x_1-x_2)(y_1-y_2)}{((x_1-x_2)^2+(y_1-y_2)^2)^{\frac{5}{2}}} - \frac{3M_bx_1y_1}{(T^2+x_1^2+y_1^2)^{\frac{5}{2}}}, \end{aligned} \tag{30}$$

$$\begin{aligned} U^0_{y_1y_1} &= \mu_1\left(n + \frac{3(1-\mu)y_1^2}{((x_1-\mu)^2+y_1^2)^{\frac{5}{2}}} - \frac{1-\mu}{((x_1-\mu)^2+y_1^2)^{\frac{3}{2}}} + \frac{3\mu y_1^2}{((x_1-\mu+1)^2+y_1^2)^{\frac{5}{2}}}\right. \\ &- \left.\frac{\mu}{((x_1-\mu+1)^2+y_1^2)^{\frac{3}{2}}}\right) + \frac{3\mu_1\mu_2(y_1-y_2)^2}{((x_1-x_2)^2+(y_1-y_2)^2)^{\frac{5}{2}}} \\ &- \frac{\mu_1\mu_2}{((x_1-x_2)^2+(y_1-y_2)^2)^{\frac{3}{2}}} + \frac{3M_by_1^2}{(T^2+x_1^2+y_1^2)^{\frac{5}{2}}} - \frac{M_b}{(T^2+x_1^2+y_1^2)^{\frac{3}{2}}}. \end{aligned} \tag{31}$$

The characteristic Equation (23) provides the eigenvalues to study the stability of the noncollinear equilibrium points in the presence of the planetesimal belt effect. The kinds of roots of Equation (23) depend on the parameters μ, μ_1, μ_2, M_b, and T. The noncollinear equilibrium points are shown in Tables 11–14 for different planetary systems. We analyzed the stability of th noncollinear equilibrium points using Equations (23)–(28), and we found that the real nonzero eigenvalues occur with opposite signs and purely imaginary eigenvalues occur with opposite signs. Thus, the noncollinear equilibrium points have a saddle$\times$center behavior.

In Figures 8 and 9, for the Sun–Saturn system with the Kuiper belt with $\mu_1 = 10^{-7}$, we plot the eigenvalues against $\mu_2 \in (10^{-10}, 10^{-7})$. Figure 8 describes the stability near L_4. Figure 8a,b presents the eigenvalues of the perpendicular equilibrium points, and Figure 8c,d depicts the eigenvalues of the inline equilibrium points near L_4. It can be observed in Figure 8a–d that real nonzero positive eigenvalues exist; thus, all noncollinear equilibrium points near L_4 are unstable in the considered system. Similarly, in Figure 9, we plot the eigenvalues of the equilibrium positions near L_5. Figure 9a,b shows the eigenvalues of the perpendicular equilibrium points, whereas Figure 9c,d depicts the eigenvalues of the inline equilibrium points. Clearly, it can be observed that at least one nonzero positive real part α of the eigenvalue exists. Thus, all equilibrium positions are unstable for the considered system.

Table 11. Perpendicular equilibrium solution near L_4 of different planetary systems.

μ	$PxL_{4-}^{P_1}$ $PxL_{4-}^{P_2}$	$PyL_{4-}^{P_1}$ $PyL_{4-}^{P_2}$	$PxL_{4+}^{P_1}$ $PxL_{4+}^{P_2}$	$PyL_{4+}^{P_1}$ $PyL_{4+}^{P_2}$
0.000286	−0.49971403464001	0.86602523034786	−0.49971396535999	0.86602535037870
	−0.49974864000649	0.86596527494152	−0.49967935999351	0.86608530578504
0.000031	−0.49996903464443	0.86602524927065	−0.49996896535557	0.86602536928619
	−0.50000364442855	0.86596530150765	−0.49993435557145	0.86608531704919
0.000000	−0.49999973464497	0.86602534317275	−0.49999966535503	0.86602546318647
	−0.50003434496569	0.86596539632081	−0.49996505503431	0.86608541003841

Table 12. Inline equilibrium solution near L_4 of different planetary systems.

μ	$IxL_{4-}^{P_1}$ $IxL_{4-}^{P_2}$	$IyL_{4-}^{P_1}$ $IyL_{4-}^{P_2}$	$IxL_{4+}^{P_1}$ $IxL_{4+}^{P_2}$	$IyL_{4+}^{P_1}$ $IyL_{4+}^{P_2}$
0.000286	−0.49971226314910	0.86602428787884	−0.49971573685090	0.86602629284772
	−0.49797714910011	0.86502280592385	−0.50145085089989	0.86702777480271
0.000031	−0.49996535971608	0.86602320762467	−0.49997264028392	0.86602741093216
	−0.49632871608103	0.86392365553369	−0.50360928391897	0.86812696302315
0.000000	−0.49998261604195	0.86601553975479	−0.50001678395805	0.86603526660443
	−0.48291574195066	0.85616197836003	−0.51708365804934	0.87588882799919

Table 13. Perpendicular equilibrium solution near L_5 of different planetary systems.

μ	$PxL_{5+}^{P_1}$ $PxL_{5+}^{P_2}$	$PyL_{5+}^{P_1}$ $PyL_{5+}^{P_2}$	$PxL_{5-}^{P_5}$ $PxL_{5-}^{P_5}$	$PyL_{5-}^{P_1}$ $PyL_{5-}^{P_2}$
0.000286	−0.49971396535999	−0.86602535037870	−0.49971403464001	−0.86602523034786
	−0.49967935999351	−0.86608530578504	−0.49974864000649	−0.86596527494152
0.000031	−0.49996896535557	−0.86602536928619	−0.49996903464443	−0.86602524927065
	−0.49993435557145	−0.86608531704919	−0.50000364442855	−0.86596530150765
0.000000	−0.49999966535503	−0.86602546318647	−0.49999973464497	−0.86602534317275
	−0.49996505503431	−0.86608541003841	−0.50003434496569	−0.86596539632081

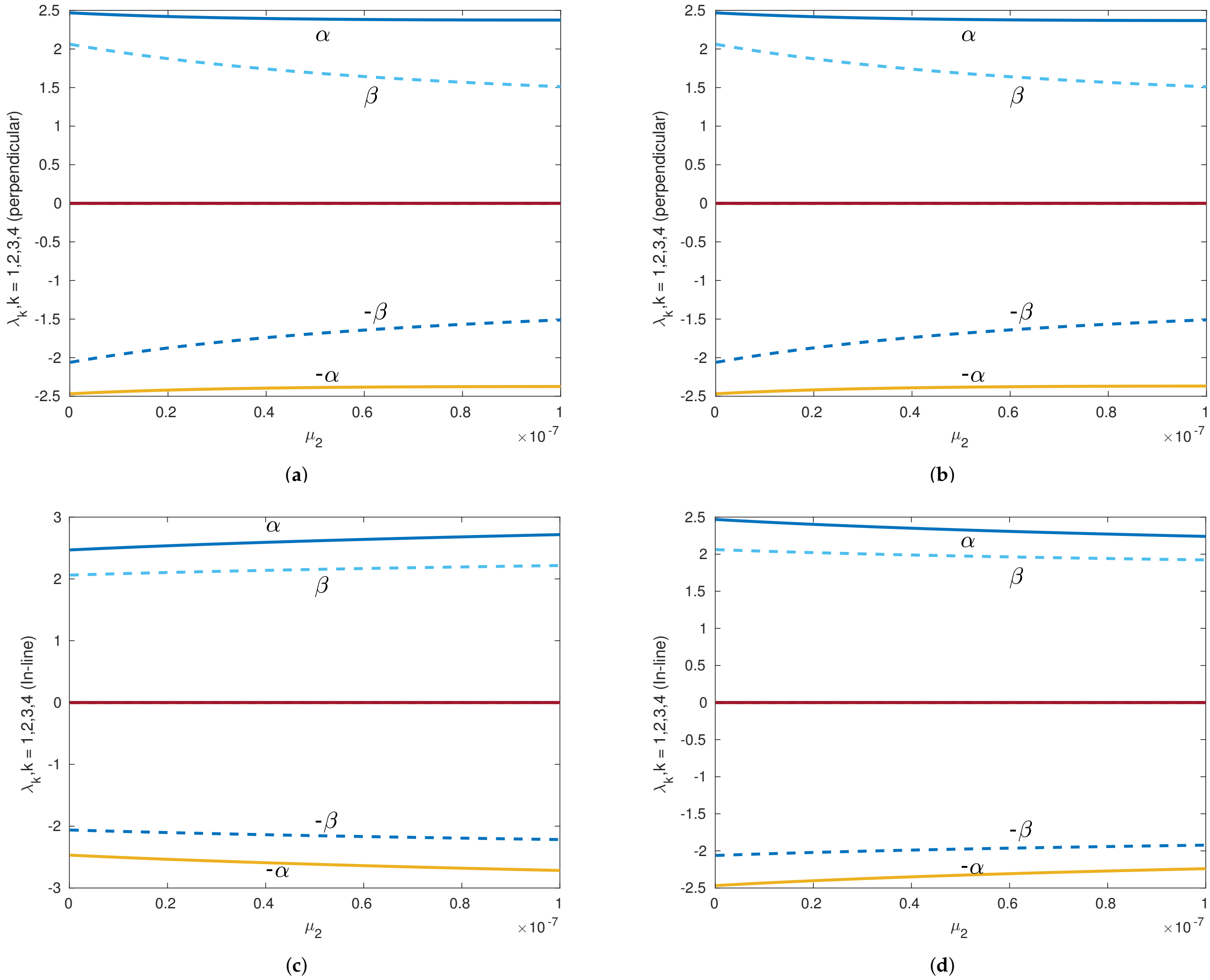

Figure 8. Eigenvalues versus $\mu_2 \in (10^{-10}, 10^{-7})$ of th Sun–Saturn system in the presence of the Kuiper belt effect near L_4 equilibrium point with $\mu_1 = 10^{-7}$. Continuous lines denote the real part of the eigenvalues, and dashed lines denote the imaginary parts of the eigenvalues for collinear points. (**a**) Eigenvalues of perpendicular equilibrium point near L_4 toward smaller primary. (**b**) Eigenvalues of perpendicular equilibrium point near L_4 away from smaller primary. (**c**) Eigenvalues of inline equilibrium point near L_4 away from center. (**d**) Eigenvalues of inline equilibrium point near L_4 toward center.

Table 14. Inline equilibrium solution near L_5 of different planetary systems.

μ	$IxL_{5+}^{P_1}$ $IxL_{5+}^{P_2}$	$IyL_{5+}^{P_1}$ $IyL_{5+}^{P_2}$	$IxL_{5-}^{P_1}$ $IxL_{5-}^{P_2}$	$IyL_{5-}^{P_1}$ $IyL_{5-}^{P_2}$
0.000286	−0.49971396535999	−0.86602535037870	−0.49971403464001	−0.86602523034786
	−0.49967935999351	−0.86608530578504	−0.49974864000649	−0.86596527494152
0.000031	−0.49996896535557	−0.86602536928619	−0.49996903464443	−0.86602524927065
	−0.49993435557145	−0.86608531704919	−0.50000364442855	−0.86596530150765
0.000000	−0.49999966535503	−0.86602546318647	−0.49999973464497	−0.86602534317275
	−0.49996505503431	−0.86608541003841	−0.50003434496569	−0.86596539632081

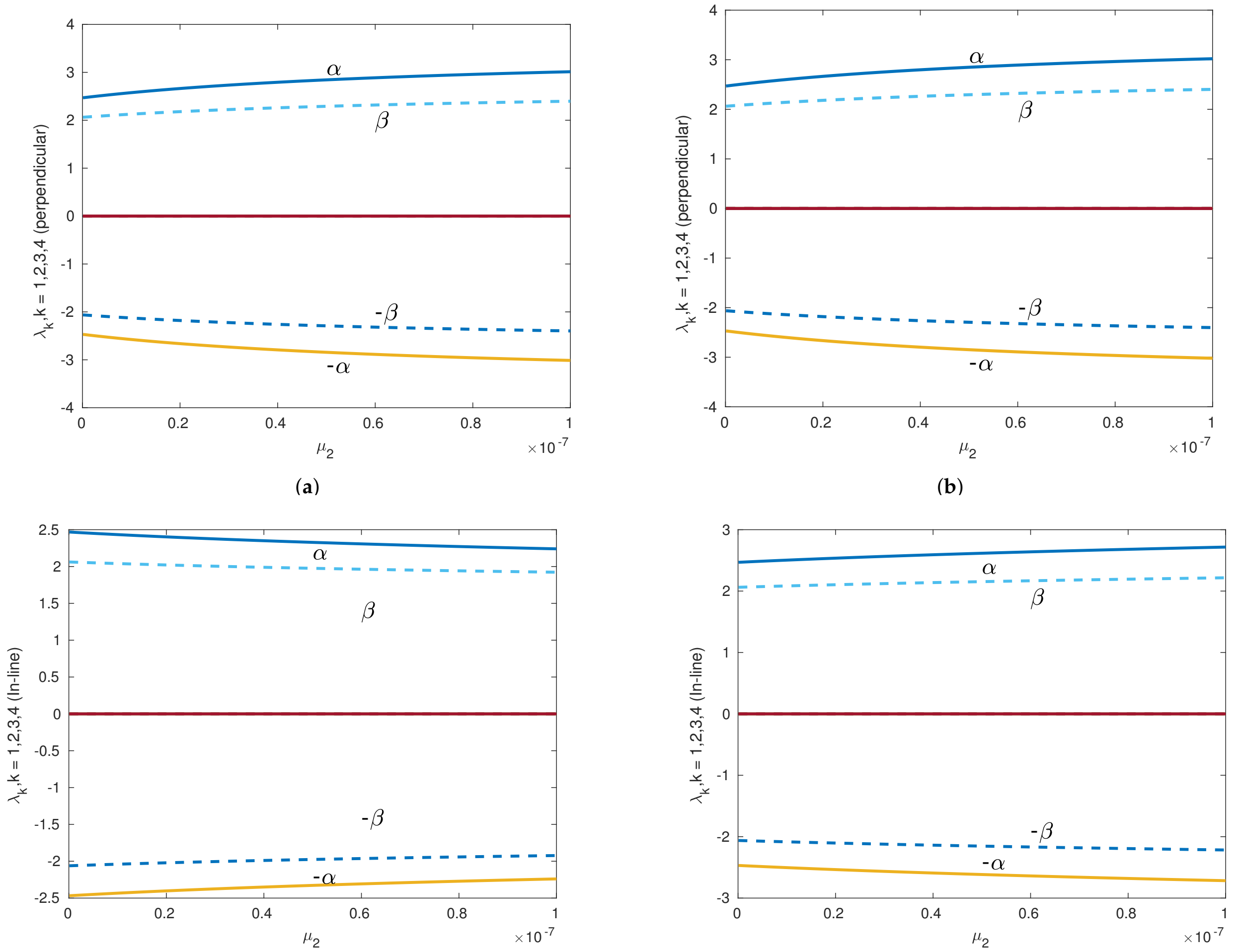

(**a**) (**b**) (**c**) (**d**)

Figure 9. Eigenvalues versus $\mu_2 \in (10^{-10}, 10^{-7})$ of the Sun–Saturn system in the presence of the Kuiper belt effect near L_5 equilibrium point with $\mu_1 = 10^{-7}$. Continuous lines denote the real part of the eigenvalues, and dashed lines denote the imaginary parts of the eigenvalues for collinear points. (**a**) Eigenvalues of perpendicular equilibrium point near L_5 toward smaller primary. (**b**) Eigenvalues of perpendicular equilibrium point near L_5 away from smaller primary. (**c**) Eigenvalues of inline equilibrium point near L_5 away from center. (**d**) Eigenvalues of inline equilibrium point near L_5 toward center.

5. Conclusions

In this study, we considered the effect of the planetesimal belt on the restricted problem of 2 + 2 bodies in a rotating coordinate system. In the absence of the planetesimal belt effect, i.e., $M_b = 0$, the proposed system coincides with the system obtained by Whipple [5]. Again, if we consider P_1 and P_2 as the single minor body, the system will convert into the CRTBP. The problem possesses 14 paired equilibrium positions around the five equilibrium points of the CRTBP. The main highlights of work can be summarized as:

- Dynamic analysis of the perturbed restricted problem of 2 + 2 bodies;
- Existence and stability analysis of both collinear and noncollinear equilibrium points;
- Description of the effect of the planetesimal belt on the motion in the proximity of equilibrium points.

The effect of the planetesimal belt on the equilibrium points and the variation in their distance from L_j, $j = 1,2,3,4,5$ were studied for some fixed parameter $M_b = 3.7 \times 10^{-7}$ and $T = 0.11$, which we compared with the unperturbed R2+2BP. For mass parameter

$\mu_1 = \mu_2 = 10^{-2}$, the distance of collinear equilibrium points $d(L_1, L_{1\pm}^{P_i})$, $i = 1, 2$ increases, and $d(L_2, L_{2\pm}^{P_i})$ and $d(L_3, L_{3\pm}^{P_i})$ decrease with the variation in μ. The distance $d(L_4, IL_{4\pm}^{P_i})$ at the inline equilibrium points increases monotonically, but the distance $d(L_4, PL_{4\pm}^{P_i})$ at the perpendicular equilibrium decreases initially for some μ. After that, it increases when μ approaches one-half. The distance of equilibrium points in the presence of the planetesimal belt effect differs from the unperturbed distance. At the collinear point, the perturbed distance d_1 is greater than the unperturbed distance d_2 at L_1 and L_3. Near L_2, $d_1 < d_2$ for $\mu < 0.153$, and $d_1 < d_2$ for $\mu > 0.153$. In the case of an inline and perpendicular equilibrium point, $d_1 > d_2$ with the variation of μ. Tables 1–3 show that the collinear equilibrium points $L_{1\pm}^{P_i}$ decrease and $L_{2\pm}^{P_i}$, $L_{3\pm}^{P_i}$ increases with the variation in $\mu \in (0, 0.5)$.

From the stability analysis, we found six paired collinear equilibrium points and eight paired noncollinear equilibrium points. The stability of all collinear equilibrium points was found to be unstable. The generalization of the stability of noncollinear equilibrium points is difficult as five different types of parameters μ, μ_1, μ_2, M_b, and T are present in the perturbed R2+2BP. The stability of noncollinear equilibrium points can be analyzed numerically. The different considered planetary systems with suitable μ_1 and μ_2 were found to be unstable.

In the framework of the perturbed restricted problem of 2 + 2 bodies by a planetesimal belt, our obtained results can be outlined as:

- The existence of equilibrium points was examined for both collinear and noncollinear points;
- The stability of motion around these points was studied;
- We compared the corresponding results of the perturbed and unperturbed models;
- The impact of a planetesimal belt was observed on collinear and noncollinear equilibrium points;
- All equilibrium points were found to be unstable, whereas the noncollinear equilibrium points were investigated numerically.

Furthermore, the restricted 2 + 2 bodies problem can be used as a credible model to describe the capture of small bodies by a planet. If the small bodies are temporarily captured in the Hill sphere of a smaller primary, they may become near enough to each other to exchange energy so that one of them becomes regularly and permanently captured.

Author Contributions: Formal analysis, G.M., A.K.P., S.A., E.I.A. and B.S.K.; Investigation, G.M., A.K.P. and B.S.K.; Methodology, G.M., A.K.P. and E.I.A.; Project administration, S.A. and E.I.A.; Software, G.M., A.K.P. and E.I.A.; Validation, G.M., A.K.P., S.A. and E.I.A.; Visualization, E.I.A.; Writing—original draft, G.M., A.K.P. and E.I.A.; Writing—review & editing, G.M., A.K.P., E.I.A. and S.A. All authors have read and agreed to the published version of the manuscript.

Funding: This research received no external funding

Institutional Review Board Statement: Not applicable.

Informed Consent Statement: Not applicable.

Data Availability Statement: The data analyzed in this study were generated by MATLAB R2018b software. The mass parameter μ of the different planetary system, the mass of the planetesimal belt M_b, and the parameter T were taken from various sources [16,23,24] and are available at the following: URL: https://nssdc.gsfc.nasa.gov/planetary/factsheet/index.html, https://ssd.jpl.nasa.gov/?phys_data (accessed on 26 December 2021).

Acknowledgments: We thank the DST(SERB) Government of India (project no. -DST(SERB)/(163)/2016-2017/506/AM) for the use of the computation facility. The first author thanks the Council of Scientific and Industrial Research (CSIR), Government of India (file no. 09/085(0126)/2019-EMR-1) for financial support. The second author thanks Manipal University Jaipur for the financial supported from the Enhanced Seed Grant through the Endowment Fund reference no. EF/2021-22/QE04-07. This work was funded by the National Research Institute of Astronomy and Geophysics (NRIAG), Helwan, Cairo, Egypt. The fourth author, therefore, thanks NRIAG for technical and financial support.

Conflicts of Interest: The authors declare that there are no conflict of interest regarding the publication of this article.

Ethics Statement: The authors state that this research complies with all ethical standards.

References

1. Pathak, N.; Abouelmagd, E.I.; Thomas, V. On higher order resonant periodic orbits in the photo–gravitational planar restricted three–body problem with oblateness. *J. Astronaut. Sci.* **2019**, *66*, 475–505. [CrossRef]
2. Pathak, N.; Thomas, V.; Abouelmagd, E.I. The perturbed photogravitational restricted three-body problem: Analysis of resonant periodic orbits. *Discret. Contin. Dyn. Syst.-S* **2019**, *12*, 849. [CrossRef]
3. Selim, H.H.; Guirao, J.L.; Abouelmagd, E.I. Libration points in the restricted three-body problem: Euler angles, existence and stability. *Discret. Contin. Dyn.-Syst.-S* **2019**, *12*, 703. [CrossRef]
4. Abouelmagd, E.I.; Guirao, J.L.G.; Llibre, J. Periodic orbits for the perturbed planar circular restricted 3–body problem. *Discret. Contin. Dyn. Syst.-B* **2019**, *24*, 1007. [CrossRef]
5. Whipple, A.L. Equilibrium solutions of the restricted problem of 2 + 2 bodies. *Celest. Mech.* **1984**, *33*, 271–294. [CrossRef]
6. Jung, C.; Zotos, E.E. Order and chaos in a three dimensional galaxy model. *Mech. Res. Commun.* **2015**, *69*, 45–53. [CrossRef]
7. Kumar, D.; Kaur, B.; Chauhan, S.; Kumar, V. Robe's restricted three-body problem when one of the primaries is a finite straight segment. *Int. J. Non-Linear Mech.* **2019**, *109*, 182–188. [CrossRef]
8. Kalvouridis, T.; Mavraganis, A. Equilibria and stability of the restricted photogravitational problem of 2 + 2 bodies. *Astrophys. Space Sci.* **1995**, *226*, 137–148. [CrossRef]
9. Kalvouridis, T. Parametric dependence of the stationary solutions in the restricted 2 + 2 body problem. *Astrophys. Space Sci.* **1998**, *259*, 77–90. [CrossRef]
10. Spurgin, G.C. Periodic orbits in the four body problem with large and small masses. *J. Differ. Equ.* **2010**, *249*, 1131–1144. [CrossRef]
11. Milani, A.; Nobili, A.M. Instability of the 2 + 2 body problem. *Celest. Mech.* **1987**, *41*, 153–160. [CrossRef]
12. El-Shaboury, S. Equilibrium solutions of the restricted problem of 2 + 2 axisymmetric rigid bodies. *Celest. Mech. Dyn. Astron.* **1990**, *50*, 199–208. [CrossRef]
13. Qi, Y.; de Ruiter, A. Orbital analysis of small bodies in co-orbital motion with Jupiter through the torus structure. *Mon. Not. R. Astron. Soc.* **2021**, *502*, 2183–2197. [CrossRef]
14. Atash, A.A.; Selim, F.; Al-Khaled, K.; Hassan, I.; Abouelmagd, E.I. Periodic orbit in the frame work of restricted three bodies under the asteroids belt effect. *Appl. Math. Nonlinear Sci.* **2020**, *5*, 157–176.
15. Singh, J.; Taura, J.J. Motion in the generalized restricted three-body problem. *Astrophys. Space Sci.* **2013**, *343*, 95–106. [CrossRef]
16. Yousuf, S.; Kishor, R. Effects of the albedo and disc on the zero velocity curves and linear stability of equilibrium points in the generalized restricted three-body problem. *Mon. Not. R. Astron. Soc.* **2019**, *488*, 1894–1907. [CrossRef]
17. Ishwar, B.; Kushvah, B. Linear Stability of Triangular Equilibrium Points in the Generalized Photogravitational Restricted Three Body Problem with Poynting_Robertson Drag. *J. Dyn. Syst. Geom. Theor.* **2006**, *4*, 79–86. [CrossRef]
18. Abouelmagd, E.I.; Awad, M.; Elzayat, E.; Abbas, I.A. Reduction the secular solution to periodic solution in the generalized restricted three-body problem. *Astrophys. Space Sci.* **2014**, *350*, 495–505. [CrossRef]
19. Miyamoto, M.; Nagai, R. Three-dimensional models for the distribution of mass in galaxies. *Publ. Astron. Soc. Jpn.* **1975**, *27*, 533–543.
20. Kushvah, B.S. Linear stability of equilibrium points in the generalized photogravitational Chermnykh's problem. *Astrophys. Space Sci.* **2008**, *318*, 41–50. [CrossRef]
21. Kumar, D.; Aggarwal, R.; Kaur, B. An insight on the restricted problem of 2 + 2 bodies with straight segment. *Astron. Nachrichten* **2020**, *341*, 669–683. [CrossRef]
22. Michalakis, D.; Mavraganis, A. The equilibrium configurations of the restricted problem of 2 + 2 triaxial rigid bodies. *Celest. Mech. Dyn. Astron.* **1995**, *63*, 81–100. [CrossRef]
23. Anglada, G.; Amado, P.J.; Ortiz, J.L.; Gómez, J.F.; Macías, E.; Alberdi, A.; Osorio, M.; Gómez, J.L.; de Gregorio-Monsalvo, I.; Pérez-Torres, M.A.; et al. ALMA discovery of dust belts around Proxima Centauri. *Astrophys. J. Lett.* **2017**, *850*, L6. [CrossRef]
24. Bixel, A.; Apai, D. Probabilistic Constraints on the Mass and Composition of Proxima b. *Astrophys. J. Lett.* **2017**, *836*, L31. [CrossRef]
25. James, J.M. *Celestial Mechanics Notes Set 4: The Circular Restricted Three Body Problem*; Florida Atlantic University, Department of Mathematical Sciences: Boca Raton, FL, USA, 2006.